Macromolecules

Article

pubs.acs.org/Macromolecules

Controlling Water Content and Proton Conductivity through Copolymer Morphology

Rasoul Narimani,[†] Ami C. C. Yang,[‡] Emily M. W. Tsang,[‡] Laurent Rubatat,[§] Steven Holdcroft,[‡] and Barbara J. Frisken*[,†]

[†]Department of Physics, Simon Fraser University, Burnaby, BC, Canada

[‡]Department of Chemistry, Simon Fraser University, Burnaby, BC, Canada

[§]UMR IPREM 5256, Université de Pau et des Pays de l'Adour, Pau, France

Supporting Information

ABSTRACT: To investigate relationships between morphology and proton conductivity in ionic copolymer membranes, we have studied two series of fluorous copolymers bearing polystyrene grafts sulfonated from 0 to 100%. Small-angle X-ray and neutron scattering experiments reveal a disordered, partially phase-separated system consisting of fluorous domains in a partially sulfonated polystyrene matrix with aggregation of ion-rich domains within the matrix. The size of the fluorous domains depends on graft density, and their packing depends on the graft chain length. The spacing of the ion-rich domains is remarkably independent of either graft chain length or charge content. We find that the samples with lower graft density, which are partially crystalline, develop a less-ordered morphology with a lower degree of phase separation. The partially crystalline samples swell less and have a slightly lower conductivity at similar water content; the lower conductivity is attributed to a more tortuous conducting phase.

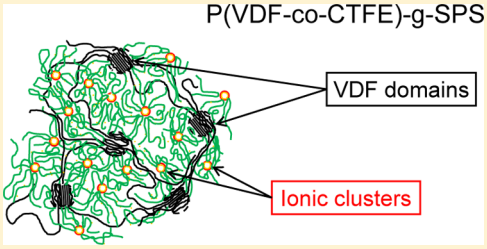

INTRODUCTION

The polymer membrane that is the heart of the proton exchange membrane fuel cell exhibits a fascinating morphology based on phase separation that both supports proton conduction and provides structural integrity. The ideal membrane should be chemically and electrochemically stable, have good mechanical strength and integrity, exhibit a high protonic conductivity, and have the potential to be prepared at low cost. A variety of ionomers have been synthesized to meet these requirements, of which Nafion, a perfluorosulfonic acid membrane, is the premier example.[1] Extensive investigation of this material has shown that phase separation between the hydrophobic polymer backbone and hydrophilic sulfonic acid groups leads to formation of interconnected, nanometer-sized ionic channels. Proton conduction occurs through these hydrophilic channels, mediated by water that is either strongly associated with the acidic groups or present as bulk water in the channels.[2]

The focus of our collaboration has been on studying the correlation between morphology, conductivity, and water uptake of proton exchange membranes (PEMs) in model polymeric systems, particularly ion-containing block copolymers. These materials can be synthesized with well-defined chain architectures, which enables systematic studies examining the correlation between chemical structure and membrane properties.[3] The combination of ion-containing and neutral blocks provides the potential of well-ordered morphologies; controlled synthesis of polymers with different architectures has led to systematic studies of relationships between morphology and physical properties important to PEM systems such as conductivity and water uptake.[4,5] While linear diblock and triblock systems are the most well-known, charge content of these systems is limited because of extreme swelling of samples when hydrated. Graft systems have the potential to develop ordered morphology while achieving greater mechanical stability. However, graft systems, specifically random graft systems, have not been investigated to the same extent, and our knowledge regarding the morphology of these materials is limited.[5,6]

We recently reported preparation of model graft system consisting of proton-conducting partially sulfonated poly([vinylidene difuoride-*co*-chlorotrifluoroethylene]-*g*-styrene) [P(VDF-*co*-CTFE)-*g*-SPS] prepared by graft-atom transfer radical polymerization of styrene from P(VDF-*co*-CTFE) macroinitiators followed by postsulfonation.[7−9] This process results in a hydrophobic fluorous backbone with ionic side chains, where both the number density and length of the side chains are controlled during synthesis. Furthermore, the charge contents of samples of a particular graft density and side chain length were varied by changing the sulfonation process; the result is a comprehensive set of samples spanning a wide region of parameter space. Comparison of results for water uptake, conductivity, and proton mobility shows that the graft system provides a membrane that is more resistant to water uptake.[7]

Received: September 27, 2013
Revised: November 27, 2013
Published: December 6, 2013

This system allows us to investigate the impact of a higher volume fraction of PS on the morphology of the membrane and to examine the effect of a different morphology class on physical properties. Previously, we studied two series of diblock copolymers consisting of sulfonated poly([vinylidene difluoride-*co*-hexafluoropropylene]-*b*-styrene block copolymers (P[VDF-*co*-HFP]-*b*-SPS),[10−12] where the PVDF is responsible for the mechanical integrity of the membrane and the SPS is the hydrophilic phase that enables proton conduction. One series consisted of a fully sulfonated PS block; the charge content was controlled by varying the length of the poly(styrene) (PS) block. This series had PS content <15 vol % in the dry phase and was characterized by a largely disordered morphology of PS domains in a PVDF matrix. The morphology is sketched in Figure 1a where the PS phase is shown in black.

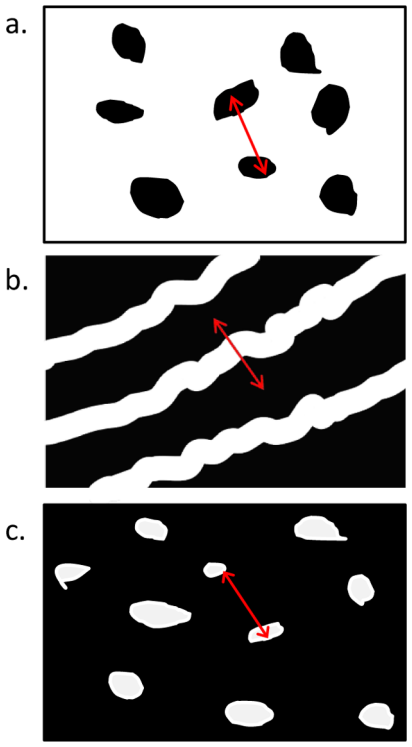

Figure 1. Morphology of PS (black) and PVDF (white) phases for systems consisting of (a) PS domains in a PVDF matrix (high PVDF content), (b) lamellar phase (roughly equal PS and PVDF content), and (c) PVDF domains in a PS matrix (low PVDF content). The arrow shows the characteristic distance between the domains in each case.

In the second series, the charge content was controlled by varying the degree of sulfonation DS of the PS block. These samples had PS content of 44 vol % in the dry phase and were characterized by a lamellar morphology (see Figure 1b). However, only limited charge content could be achieved because the diblock samples with higher SPS content were subject to extreme swelling.

In this paper we report a structural study of samples from two series with different graft densities. The PS content for all samples is at least 64 vol % in the dry phase and as high as 92 vol %. We expect these samples to consist of PVDF domains in PS matrix (see Figure 1c), allowing us to study a significantly different, but complementary morphology. Furthermore, study of these polymers is motivated by similarities to the architecture of Nafion, the most widely used PEM material, which consists of a tetrafluoroethylene backbone and short side chains, each bearing a single ionic group.

In both our previous work on the graft system[7−9] and that of Zhang et al. on a similar system,[13] the morphology of the graft system was investigated by transmission electron micrography of samples stained with lead acetate. This method reveals the ion-rich regions of the dry sample but cannot differentiate between regions rich in unsulfonated PS and those rich in PVDF.

In this work, we use small-angle X-ray (SAXS) and small-angle neutron scattering (SANS) to definitively probe the morphology of the system. X-ray and neutron scattering are sensitive to the electronic and scattering length densities of materials, respectively. Therefore, these techniques provide very powerful, and complementary, tools to study the phase separation and morphology of soft materials including polymeric systems.[14,15] We present results of SAXS measurements on dry samples and SANS measurements of hydrated samples. We first focus on size and separation of the fluorous domains in the unsulfonated samples and subsequently discuss the effect of sulfonation and hydration on these parameters. We investigate the morphology of the ion-rich regions in the hydrated domains. Finally, we discuss how the nanoscale characteristics revealed by scattering are correlated to the water content and conductivity of the polymer membranes.

MATERIALS AND METHODS

Materials and Bulk Properties. Figure 2 illustrates the chemical structure of the polymers studied. Two series of graft copolymers were

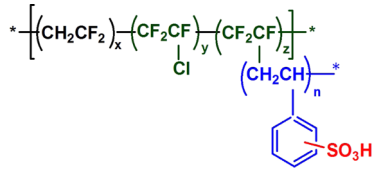

Figure 2. Chemical structure of poly([vinylidene diflouride-*co*-chlorotrifluoroethylene]-*g*-styrene).

made based on two macroinitiators obtained by polymerization of PVDF and CTFE. CTFE monomers and hence graft points are located randomly along the backbone. Details of the synthetic pathway and membrane preparation are described elsewhere.[8,9] To summarize, these two series are identified by their graft number densities, 1.7% and 2.5%, defined by the fraction of monomers in the backbone to which SPS side chains are attached, and in this paper we refer to samples with lower (LGD) and higher graft number density (HGD), respectively. As demonstrated in Table 1, in each series samples are available with three different lengths of side chain *n*, namely short, medium, and long. Each of these samples was sulfonated to a different degree ranging from 0 to even 100% in some cases. Membranes ≈100 μm thick were obtained by solution casting; the polymer was dissolved in *N*,*N*-dimethylacetamide to form a slightly viscous solution, and a drop of the solution was spread on a Teflon sheet, where the size of the drop determined the area and thickness of the film. The samples were covered and dried slowly at room temperature for 2 days and further dried overnight at 60 °C in order to remove any residual solvent. Membranes were protonated by immersion in 2 M HCl for at least 4 h. The protonated membranes were rinsed with deionized water to remove any excess acid on the surface of the membranes.

The degree of sulfonation DS, water uptake, ion-exchange capacity IEC, number-average molar mass and polymerization degree of these samples were measured previously. Methods and results are described in detail in previous papers.[8,9] Definitions of these terms as used in this

dx.doi.org/10.1021/ma402008b | *Macromolecules* 2013, 46, 9676−9687

Table 1. Polymer Architecture of the Unsulfonated Graft Copolymers[7−9]

series	CTFE[a] (%)	x	y	z[b]	GD[c] (mol %)	m[d]	n	w_{PVDF}[e] (mass %)	ϕ_{PVDF} (vol %)	ρ_{unsulf}[f] (g/cm^3)
LGD							39	49	36	1.32
	2.6	1830	17	32	1.7	59	62	38	26	1.25
							79	31	21	1.21
HGD			164	105	2.3	43	35	46	33	1.30
	5.8	4375	151	119	2.6	38	88	22	14	1.16
			151	118	2.7	37	154	13	8	1.11

[a]Amount of CTFE in the macroinitiator CTFE = $[(y + z) \times 100\%]/(x + y + z)$. [b]$x$, y, z, and n are defined as shown in Figure 1. [c]Graft number density GD = $(z \times 100\%)/(x + y + z)$. [d]Average number of monomers on the backbone between grafts. [e]The mass fraction of the sample occupied by PVDF backbone $w_{PVDF} = (M_{PVDF} \times 100\%)/(M_{PS} + M_{PVDF})$, where M_{PS} is the mass of polystyrene and M_{PVDF} is the mass of P[VDF-*co*-CTFE] in the polymer. [f]Mass density of the unsulfonated copolymer, calculated using eq S6, which can be found in the Supporting Information.

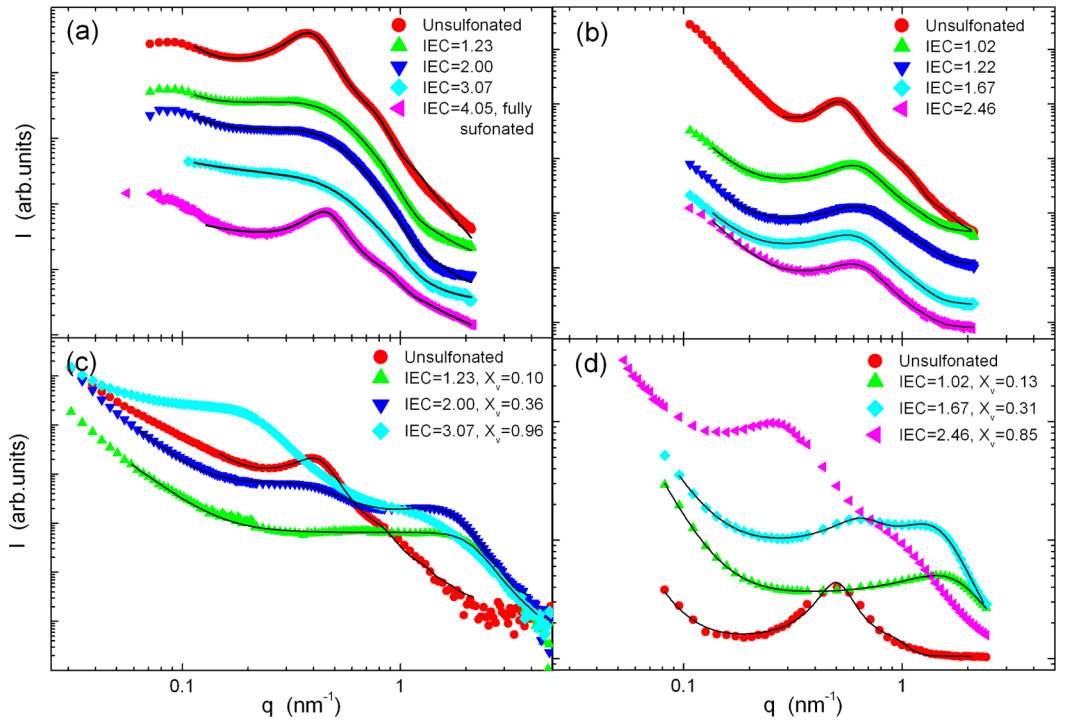

Figure 3. Scattering data for samples with medium length grafts. (top row) SAXS intensity as a function of scattering wave vector for samples with different degrees of sulfonation for (a) LGD series with medium (n = 62) graft chain lengths and (b) HGD series with medium (n = 88) graft chain lengths. (bottom row) SANS intensity as a function of scattering wave vector for samples with different degrees of sulfonation (c) LGD medium (n = 62) and (d) HGD medium (n = 88) graft chain lengths. Samples for SAXS were dry; samples for SANS were hydrated with D_2O. The solid line on each data set shows the result of fitting eq 6 to the data. Background scattering has been subtracted, and data sets have been shifted vertically for clarity.

paper can be found in the Supporting Information, which also includes a table summarizing results for the degree of DS, IEC, and X_v for the samples used in this study (Table S2). In this study, the term "water content" refers to a volume-based water content X_v and is defined as

$$X_v = \frac{V_{wet} - V_{dry}}{V_{wet}} \quad (1)$$

where V_{wet} and V_{dry} are the volume of the hydrated and dry samples, respectively.

The samples were imaged using transmission electron microscopy (TEM).[8,9] Samples were stained by soaking in lead acetate solution, dried, embedded in epoxy, and sectioned to yield sections 60−100 nm thick. Images revealed a disordered phase-separated morphology. Dark regions, 2−4 nm in size, were interpreted as being ion-rich regions as the stain is expected to accumulate in these areas.

We have also studied the crystallinity of these samples through wide-angle X-ray scattering measurements on dry samples. We observe crystallinities up to 12% in samples of the LGD series with short side chains and of up to 6% in samples of the LGD series with medium and long side chains.[9] The crystallinity was largely independent of sulfonation, except that the unsulfonated sample with short side chains was only 6% crystalline. In contrast, crystallinity in the HGD series was too small to measure.[8] We also studied the crystallinity of the macroinitiator, P(VDF-*co*-CTFE), as a function of the CTFE mole ratio with the CTFE ratio varying from 0 to 0.056. We found that the crystallinity decreased from 32 to 12% as the CTFE mole ratio increased.[16] Thus, we associate the higher crystallinity of the former series to the lower CTFE ratio and subsequent lower GD.

Small-Angle X-ray Scattering. Small-angle X-ray scattering (SAXS) measurements were obtained with two instruments: a Bruker Nanostar SAXS instrument located at National Institute of Nanotechnology in Edmonton, Alberta, and a Rigaku S-MAX located at the Adolphe-Merkle Institute in Fribourg, Switzerland. In both cases, the X-ray wavelength was 1.54 Å. In order to decrease the scattering due to air molecules, the volume between the source and detector, including the sample holder, was maintained at low pressure (2×10^{-2} bar). Data were acquired in transmission mode on a 2-D detector. We obtained SAXS measurements on five different spots on each sample

dx.doi.org/10.1021/ma402008b | *Macromolecules* 2013, 46, 9676−9687

to check sample uniformity. For further analysis we used the sum of the five different runs.

Small-Angle Neutron Scattering. Neutron scattering experiments were performed on D11 at the Institut Laue-Langevin in Grenoble, France. The neutron wavelength selected was 6 Å, and three sample−detector distances were used: 1.2, 5.5, and 20.5 m. The samples were contained in cells with quartz windows, with a gap of 1 mm between the two windows; the remaining space was filled with water. The samples were maintained at ambient temperature during measurement. The technique of neutron scattering was chosen to take advantage of the contrast variation method. To vary the scattering contrast between the polymer matrix and the solvent, the membrane was soaked in four different H_2O and D_2O mixtures: H_2O, 30−70 (30% D_2O, 70% H_2O), 60−40 (60% D_2O, 40% H_2O), and finally D_2O. These mixtures have scattering length densities (SLD) of -0.56×10^{10}, 1.52×10^{10}, 2.91×10^{10}, and 6.37×10^{10} cm cm^{-3}. We have estimated the SLD of PVDF and PS to be 2.87×10^{10} and 1.41×10^{10} cm cm^{-3}.[17]

EXPERIMENTAL RESULTS

Data from SAXS and SANS Measurements. The two-dimensional scattering spectra are isotropic, and azimuthal averages of the data are shown in Figure 3 for samples with medium-length side chains. Figures 3a and 3b show SAXS data for samples from the LGD and HGD series, respectively. The scattered intensity I decreases gradually as q increases from 0.1 to 2 nm^{-1}, where $q = \frac{4\pi}{\lambda}\sin(\theta)$ is the scattering wave vector, λ is the wavelength of the radiation and θ is the scattering angle. It contains one main peak at q^* with evidence of a secondary peak in some samples, particularly in samples where the PS side chains are either unsulfonated or fully sulfonated. Because the secondary peak is located at $q \approx 2q^*$, we interpret this as a second-order peak that indicates that these samples have a more ordered morphology. In general, the main SAXS peak for medium and long graft chain length samples is located at a lower q than that for short graft chain length samples. For example, the main peak position for unsulfonated samples with long and medium side chains in the LGD series is located at $q^* \approx 0.35$ nm^{-1}, while the peak position for the unsulfonated short side chain sample is located at $q^* \approx 0.45$ nm^{-1}. In the partially sulfonated samples, the main peak is broader and the secondary peak is less pronounced, indicating a less ordered morphology. The samples with the broadest peaks with lowest amplitude are the partially sulfonated LGD samples with short side chains (data not shown).

These SAXS spectra are characteristic of nanosize domains with weak ordering. The samples are not stained or hydrated; therefore, characteristic features corresponding to ion-rich or water-rich domains are not visible in the SAXS data,[14,15] and the scattering is due to contrast between fluorous and polystyrene-rich domains. We associate the peak in the scattering data with short-range order between domains of PVDF in a polystyrene-rich matrix because the PVDF occupies a smaller volume fraction than the PS/SPS component; as shown in Table 1, the PVDF volume fraction is less than 36% even for dry samples. In unsulfonated or fully sulfonated samples, the contrast is between PVDF and PS or PVDF and SPS, respectively. In partially sulfonated samples, the situation is more complicated as there is also the possibility of separation into three phases: PVDF-rich, PS-rich, and SPS-rich.

Figures 3c and 3d show SANS data for samples from the LGD and HGD series, respectively, where samples were hydrated in D_2O. There is significant variation between spectra from samples with different degrees of sulfonation. Scattering from the unsulfonated sample is consistent with SAXS measurements of the same sample, but in the low IEC sample from both series (IEC = 1.23 and 1.02 mmol/g in LGD and HGD samples, respectively) this peak disappears and a second peak at higher q, $q^* \approx 1.5$ nm^{-1}, emerges. The higher IEC samples all show two peaks; in the highest IEC samples the first peak shifts to lower q, consistent with swelling of the membrane; at this point the water content of the LGD and HGD samples are 96 and 85%, respectively.

Neutron scattering spectra have been measured for membranes soaked in four water mixtures. Spectra for the LGD samples with medium-length side chains with IEC = 2.00 mmol/g are shown in Figure 4. Varying the isotope

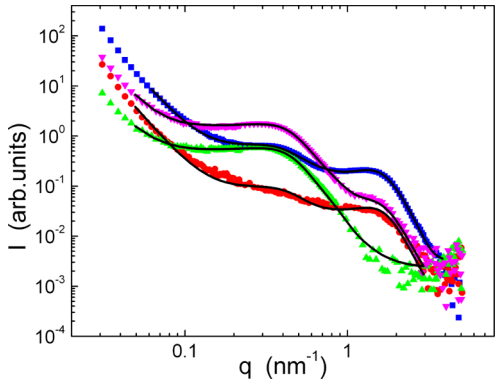

Figure 4. SANS spectra for the LGD sample with medium-length side chains and IEC = 2.00 mmol/g hydrated in four water mixtures: ■, D_2O; ▼, H_2O; ●, 60−40 mixture; ▲, and 30−70 mixture. The water content of this membrane was 0.36. The solid line on each data set shows the result of fitting eq 6 to the data. Data sets have been shifted vertically for clarity.

composition of the water has an effect on each of the two main peaks, changing the relative amplitude and even making one or the other peak completely disappear. For example, peak 1 disappears in the 60−40 mixture, and peak 2 disappears when the sample is hydrated in the 30−70 mixture. This behavior is consistent with a three-phase system consisting of PVDF domains in a matrix consisting of PS-rich and SPS-rich regions. Assuming the water concentrates in the ion-rich regions of the sample, the water changes the overall scattering length density of the PS matrix. In the case of the 60−40 mixture for this sample, the amount of water absorbed and its SLD are sufficient to increase the SLD of the matrix enough to match that of the PVDF domains, causing the PVDF structure to disappear and confirming our observations from the SAXS measurements that the first peak can be attributed to the PVDF structure. In the case of the 30−70 mixture, the SLD of this solvent matches that of PS. This reduces contrast between the regions of SPS and PS; since peak 2 disappears for all samples hydrated with this mixture, we associate peak 2 with the morphology of the ion-rich domains. This peak can be compared to the "ionomer peak" commonly observed in these systems.[15] Consistent with the picture, we observe that peak 2 is absent in the unsulfonated samples, which are uncharged and do not absorb any water.

Modeling of the Scattering Data. Our data are consistent with a structure consisting of fluorous or PVDF domains in a polystyrene matrix. The polystyrene matrix consists of regions of sulfonated and unsulfonated polystyrene; when hydrated, the solvent accumulates in regions high in SPS. There will be some

dx.doi.org/10.1021/ma402008b | Macromolecules 2013, 46, 9676−9687

PVDF in the PS phase because of geometric constraints: the PVDF is attached to the PS side chains. Also, we know that the domains are connected because water swelling is controlled and is considerably less than diblock samples of the same material.

In order to interpret the spectra, we use a fitting function with two main terms: one designed to describe the morphology of the fluorous domains and the other that of the water-rich domains. A schematic of the model described by the fitting function is shown in Figure 5. The main features of the fitting function are described below; details can be found in the Supporting Information.

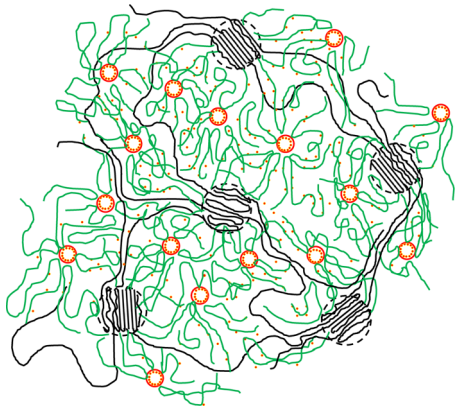

Figure 5. Schematic of the model used to describe the morphology of the graft copolymer membranes. The backbones of the graft copolymers (black) order to form interconnected PVDF domains, which are approximated as polydisperse spheres embedded in a continuous PS matrix (green). In the graft architecture, side chains are chemically bound to the backbone. At shorter length scales, structure due to ion-rich domains within the PS matrix is visible. This sketch represents a dry membrane, and we have shown ion-rich domains (yellow and red) as individual clusters. Regions of higher SPS content absorb solvent as the membrane is hydrated, providing continuous channels for proton conduction.

To describe the peak at lower q, due to the morphology of the fluorous domains, we use a model proposed by Kinning and Thomas[18] (KT model) to describe a disordered arrangement of quasi-spherical domains in diblock copolymers. The model consists of a form factor for polydisperse spheres with liquid-like order as described by the Percus–Yevick correlation function.[19] The spheres are assumed to be surrounded by a shell or corona that limits the minimum distance between them so that the distance of closest approach is larger than twice the radius of the spheres. We picture the spheres as a description of higher density or crystalline PVDF domains and the corona being due to PS grafts attached to the backbone. Our choice of model function was partly motivated by variation in the PVDF peak between samples. In particular, it is narrower and accompanied by a second-order peak in the data of the unsulfonated and fully sulfonated samples, indicating that these samples have more developed and ordered morphologies as compared to the partially sulfonated samples. The KT model captures this liquid-like order in samples with a low degree of order and has been used to follow phase separation in asymmetric diblock copolymers, for example.[20] Other model functions used, such as the Teubner–Strey model,[21] did not provide an adequate fit to the data. Peaks at q and $2q$ can also indicate a lamellar structure, but there was no indication of lamellar structure in TEM images.[8,9] A lamellar structure is also not consistent with the volume fractions of fluorous and polystyrene components, where lamellar structures are expected when the volume fractions are roughly 50%; the maximum volume fraction of the fluorous component is 36% in the short graft chain length LGD samples.

In the KT model, the q-dependence of the scattered intensity is expressed as a product of the form factor for polydisperse spheres $P(q; R_C, \sigma)$ and a structure function $S(q; R_{HS}, \phi_{HS})$ describing their short-range order

$$I_{KT}(q; R_C, \sigma, R_{HS}, \phi_{HS}) = P(q; R_C, \sigma)S(q; R_{HS}, \phi_{HS}) \quad (2)$$

where R_C is the average size of the fluorous domains, σ is the standard deviation of the domain size distribution, $2R_{HS}$ is the distance of closest approach of the domains, where the hard-sphere radius R_{HS} is roughly the radius of the fluorous core and the surrounding shell, and finally ϕ_{HS} is the hard-sphere volume fraction. We have used the Schulz distribution to describe the dispersity.[22] The hard-sphere volume fraction ϕ_{HS} can be expressed in terms of the hard-sphere volume V_{HS} and the domain number density n_D

$$\phi_{HS} = V_{HS}n_D \quad (3)$$

where

$$V_{HS} = \frac{4\pi}{3}{R_{HS}}^3 \quad (4)$$

To describe the peak at higher q that is evident in the hydrated samples, we chose a model that describes irregularly shaped domains with short-range order: the Teubner–Strey model (TS model).[6,21,23] The TS model has two parameters defining two typical lengths: a characteristic separation length of the domains d and a correlation length ξ that describes the extent of the correlation of the domain arrangement

$$I_{TS}(q; d, \xi) = \frac{8d^4\pi}{\xi[16\pi^4 + 8d^2\pi^2(\xi^{-2} - q^2) + d^4(\xi^{-2} + q^2)]} \quad (5)$$

We also tried using an additional KT term to fit the data but found that the fits were not improved and the data did not support the use of the additional parameters.[16] As seen by other authors,[23] both forms fit the peak associated with the water-rich domains very well.

Two additional terms were added to finalize the fitting function. All the data show an upturn at low q, most likely due to large length scale density fluctuations in the samples.[24] We used an additional term consisting of a power law with an exponent of −4 in order to accommodate this behavior. Other models such as the Debye–Buche model[25] were considered as descriptions of this behavior but did not provide additional insight due to the q-range probed in these experiments. With the addition of a constant background, the final fitting function is written

$$I(q; A_0, A_1, A_2, A_3, R_C, \sigma, R_{HS}, \phi_{HS}, d, \xi) = A_0 + A_1q^{-4} + A_2I_{KT}(q; R_C, \sigma, R_{HS}, \phi_{HS}) + A_3I_{TS}(q; d, \xi) \quad (6)$$

in which A_0, A_1, A_2, and A_3 are the amplitudes of the background, power law, Kinning–Thomas, and Teubner–Strey terms, respectively. A_3 was set to zero when fitting to spectra for

dx.doi.org/10.1021/ma402008b | Macromolecules 2013, 46, 9676–9687

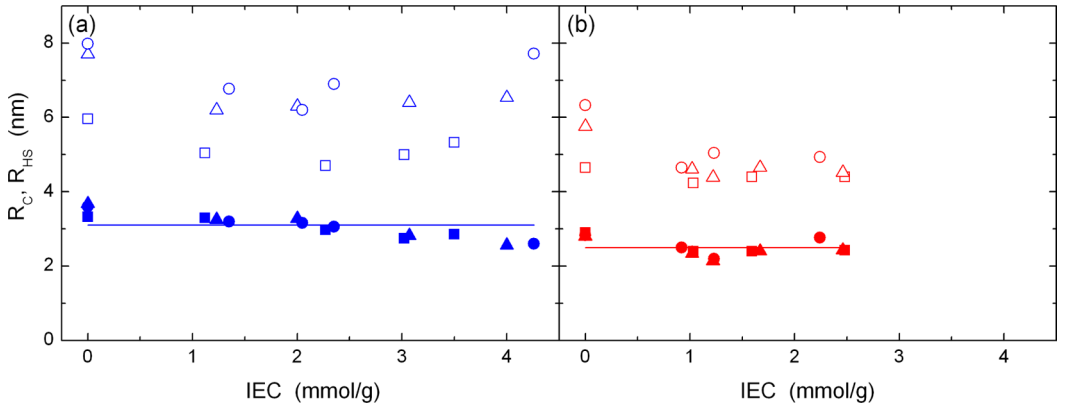

Figure 6. Parameters obtained by fitting the model function eq 6 to the SAXS data for (a) LGD and (b) HGD samples. Results for the radius of the fluorous core R_C and the hard-sphere radius R_{HS} are shown as filled and open symbols, respectively. Different symbol shapes are used for samples of different graft chain length: short (squares), medium (triangles), and long (circles). The straight line indicates the average size of R_C for the two series. Parameter uncertainties are shown as error bars if they are larger than the symbol size.

unsulfonated or nonhydrated samples. This model was successfully fit to all SAXS data and to SANS data for samples with water content <80%. Samples with higher water content are highly swollen and flexible with a gel-like appearance; they are characterized by a clearly different scattering pattern as seen in Figure 3 for the highest IEC samples. Figures 3 and 4 contain curves that represent the results of fitting eq 6 to the data.

To check our model of PVDF domains in a PS matrix, we have compared the amplitudes A_2 and A_3 of eq 6 for samples hydrated in different water mixtures. The amplitudes should be proportional to the contrast factor, which varies as the square of the difference in scattering length density between the structure and its surroundings. For A_2, the contrast is between the PVDF domain and the surrounding matrix consisting of PS and SPS and solvent and possibly PVDF. For A_3, the contrast is between the solvent and the surrounding matrix, consisting of SPS, PS, and possibly PVDF. We find good agreement between ratios of A_2 and A_3 for fits from samples hydrated in different water mixtures if we assume that all of the PVDF is in the domains. However, we know that there has to be some PVDF outside the domains because interconnection of the PVDF-rich regions is what holds the membrane together. Consistency of the contrast amplitudes is more likely telling us that the PVDF stays away from the ion-rich regions—these features could be examined in a more detailed model. Details of our analysis of the contrast amplitudes can be found in the Supporting Information.

Fluorous Domains. Figures 6a and 6b compare the parameters R_C (solid symbols) and R_{HS} (open symbols) obtained from fits to the SAXS data for dry samples from both series for samples of different charge content expressed in terms of the IEC. In both series, the radius of the domains is independent of graft chain length, but it does depend on graft density. The radius of the fluorous core R_C is larger in samples from the LGD series; the average size of R_C for the LGD series is 3.10 ± 0.06 nm while that of the HGD series is 2.50 ± 0.07 nm (solid lines). The radius of the fluorous domains R_C decreases slightly as the degree of sulfonation is increased in the LGD series; no change is apparent in the HGD series. The dispersity σ was generally 30% for all samples.

We interpret the difference in domain size to mean that the size of the fluorous domains is related to the distance between graft points. The average number of monomers between grafts is an important parameter in graft polymeric systems; m values for our samples are included in Table 1. For the LGD series, m = 59 while m = 39 for the HGD series; the ratio between these two values is 1.5, while the ratio of average R_C values for the two series is 1.24. The average core sizes $2R_C$ are 6.2 and 5.0 nm, about half that expected for the distance between graft points, estimated based on an intermonomer spacing of 0.23 nm for PVDF,[26,27] of 13.6 and 9 nm between graft points for the LGD and HGD series, respectively. Given that graft locations are random along the backbone resulting in dispersity in the distance between grafts, both the size ratios and the absolute values compare favorably.

While the size of the fluorous domains appears to be largely independent of the length of the side chain, this is not the case for the distance of closest approach. For unsulfonated samples, the samples with medium and long side chains have larger R_{HS} than the short side chain samples, with R_{HS} slightly larger for the longer side chain in both cases. The distance of closest approach also decreases slightly as the degree of sulfonation increases. Among sulfonated samples, R_{HS} of the LGD samples with medium and long graft chain lengths are 30% higher than R_{HS} for the short graft chain length samples. These observations are consistent with behavior of linear diblocks, where the distance of closest approach was found to scale with block length.[28] This trend is not apparent in the HGD series; all of the high graft density samples have similar R_{HS}.

Differences between Local and Macroscopic Swelling. Figure 7 compares results of fitting eq 6 to SAXS and SANS data for LGD samples. SAXS measurements were made on dry samples, in vacuum, while SANS measurements were made on samples swollen in the 30−70 solvent mixture. The parameters R_C and R_{HS} obtained in the fits are compared for the hydrated (open, blue symbols) and dry (filled, blue symbols) samples. Figure 7a shows that the size of the fluorous core does not change when the samples are hydrated. Figure 7b shows that the distance of closest approach between domains is comparable in hydrated and dry unsulfonated samples, which do not absorb water, and slightly larger in the hydrated partially sulfonated samples at low IEC, IEC < 1.5 mmol/g. At higher IEC values the distance of closest approach increases significantly.

We can check for differences between local and macroscopic swelling by comparing measured values for the volume of the domain consisting of fluorous core and shell V_{HS} to values calculated based on each sample's water uptake. The hard-sphere volume of the swollen samples V_{HS}^{wet} can be calculated

dx.doi.org/10.1021/ma402008b | *Macromolecules* 2013, 46, 9676−9687

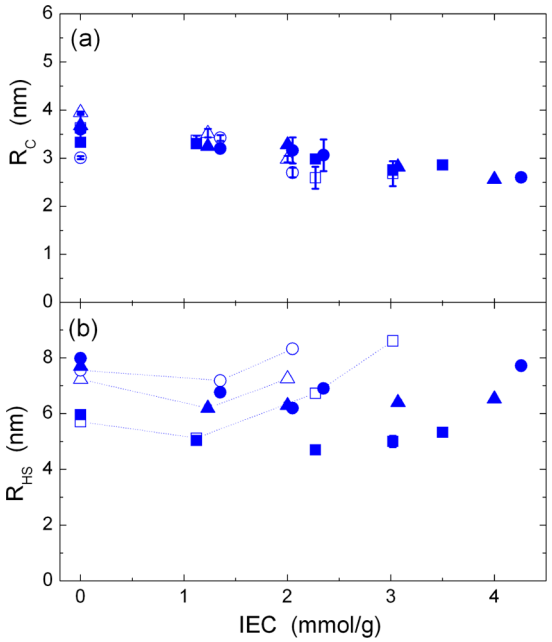

Figure 7. Comparison of (a) the radius of the fluorous core and (b) hard-sphere radius obtained by fitting the model function eq 6 to SAXS (filled symbols) and SANS data (open symbols) for samples from the LGD series. Samples for SANS have been hydrated in the 30−70 solvent while samples for SAXS are measured in vacuum. Different symbol shapes are used for samples of different graft chain length: short (squares), medium (triangles), and long (circles). Parameter uncertainties are shown as error bars if they are larger than the symbol size.

directly from SANS measurements of the hydrated samples using eq 4. We can also calculate V_{HS}^{wet} from the hard-sphere volume in the dry sample V_{HS}^{dry} and the measured water content X_v

$$V_{HS}^{wet} = \frac{V_{HS}^{dry}}{1 - X_v} \tag{7}$$

where the volume of the fluorous core and its shell for dry samples is obtained using R_{HS} determined from SAXS measurements of the dry samples. We find that these values agree within 10% for all samples with $X_v < 0.8$. Figure S1 in the Supporting Information compares the results. The fact that the volume of the fluorous domains grows at a rate consistent with the water uptake indicates that swelling on microscopic length scales is consistent with macroscopic behavior.

Phase Separation. Results for the hard-sphere volume fraction, the parameter that indicates the degree of liquid-like order in the system, can be found in Figure 8, where the results are plotted as a function of the charge content or IEC of each sample. The hard-sphere volume fraction decreases with charge content, with the HGD samples generally having a higher ϕ_{HS} than the LGD samples. The parameter ϕ_{HS} increases at high IEC for the samples in LGD series that are fully sulfonated; fully sulfonated samples with medium and long side chains possess the highest ϕ_{HS} values among all sulfonated samples. This trend in the value of ϕ_{HS} is consistent with the data that show a secondary peak that is stronger in the unsulfonated and fully sulfonated samples and generally more evident in the HGD. In the hard-sphere model, a larger hard-sphere volume fraction indicates a more ordered system. This parameter has also been used to describe the degree of phase separation by

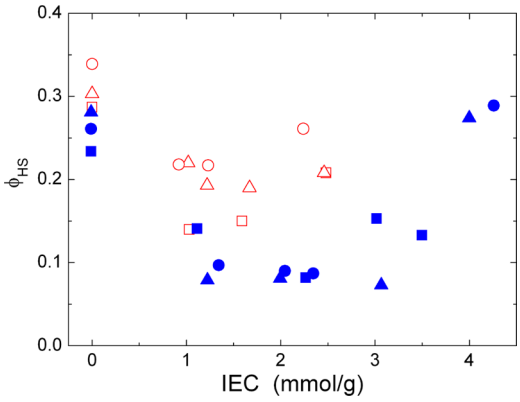

Figure 8. Values found for the hard-sphere volume fraction of the fluorous domains obtained by fitting the model function eq 6 to the SAXS data for LGD (short, ■; medium, ▲; and long, ●) and HGD (short, □; medium, △; and long, ○) series of polymer membranes as a function of charge content expressed as the IEC.

various authors.[29] These results indicate that the unsulfonated and fully sulfonated samples have a higher degree of order and phase separation than the partially sulfonated samples and that the LGD samples are less ordered than the HGD samples.

To quantify the degree of phase separation, we estimate how much of the fluorous backbone participates in the PVDF domains. The ratio f of the volume occupied by the fluorous cores to the volume of PVDF available in the sample is

$$f = \frac{\phi_C}{\phi_{PVDF}} = \frac{\frac{R_C^3}{R_{HS}^3}\phi_{HS}}{\phi_{PVDF}} \tag{8}$$

where ϕ_{PVDF} is the volume fraction of PVDF in the sample, calculated using eq S10. If all of the PVDF were to be incorporated into the domains, i.e., phase separation was complete, we would expect this ratio to be 1. Figure 9 shows

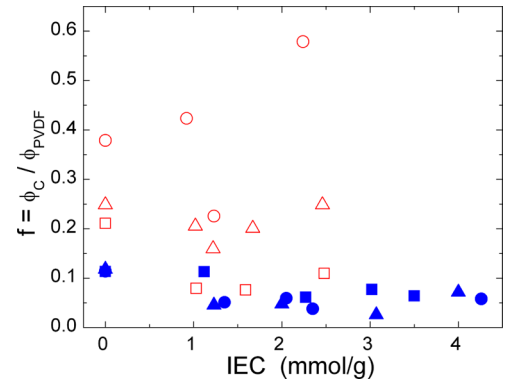

Figure 9. f, the volume fraction of the backbone contributing to the formation of fluorous domains, is calculated using eq 8. LGD (short, ■; medium, ▲; and long, ●) and HGD (short, □; medium, △; and long, ○) series of polymer membranes as a function of charge content expressed as the IEC.

the values obtained for two series as a function of the IEC. Values of f range from lows of 3% to highs of almost 60%. They are generally smaller in the LGD series, where roughly 10% of the PVDF participates in the fluorous domains for the samples that are partially sulfonated. In the HGD series, the phase separation is improved by increasing the length of the side

dx.doi.org/10.1021/ma402008b | *Macromolecules* 2013, 46, 9676−9687

chains, with the longest side chain sample being characterized by significant phase separation. This is consistent with phase separation in conventional copolymers, where phase separation depends on the molar mass of the different components.

The lower degree of phase separation in the LGD series can be attributed to the fact that these samples are more crystalline: hindrance of phase separation due to crystallinity has been reported in both general[30] and graft[31] copolymers. The formation of crystalline domains is believed to induce kinetically trapped domains in the system such that the system may never reach the equilibrium state.[30] The fact that f is similar in all samples in this series suggests that the crystallinity dominates the phase separation in this case.

The lower degree of phase separation in the partially sulfonated samples, which is particularly apparent in the data for ϕ_{HS} for the LGD samples, can be attributed to increased complexity. In the case of sulfonated samples, phase separation is determined by two contributions: the segregation of fluorous segments and the aggregation of ionic domains. When the samples are partially sulfonated, the acid groups are located randomly along the side chains. We suspect that the aggregation of the ionic groups in the partially sulfonated samples competes with phase separation of fluorous and polystyrene phases and that the random distribution of the acid groups along the side chains diminishes long-range order between the fluorous domains. This is somewhat different from diblock systems, where a moderate level of sulfonation tends to increase order[12,32] while only very high degrees of sulfonation result in decreased long-range order.[8]

Ion-rich Domains. Fits of the TS model function to the higher-q peak in the SANS spectra result in two length scales: the spacing between the ion-rich domains d and a length scale ξ that describes how correlated the domains are. Results are shown in Figure 10 as a function of the water content of the samples. The domain spacing is remarkably similar for 9 of the 12 samples, even though side chain length is varying from 39 to 154 monomers and distance between grafts is varying from 37 to 59 monomers. While recent experiments[8] and simulations[33] on dry membranes have suggested a difference in size of ion-rich regions as polymer architecture is varied, this behavior is not evident here. There is a slow growth of this length scale with water content; as the water content varies from roughly 10 to 80%, the domain spacing increases from 4 to 4.5 nm. The correlation length is quite short, does not vary much between samples, and is roughly independent of water content. It has an average value of 1.5 nm.

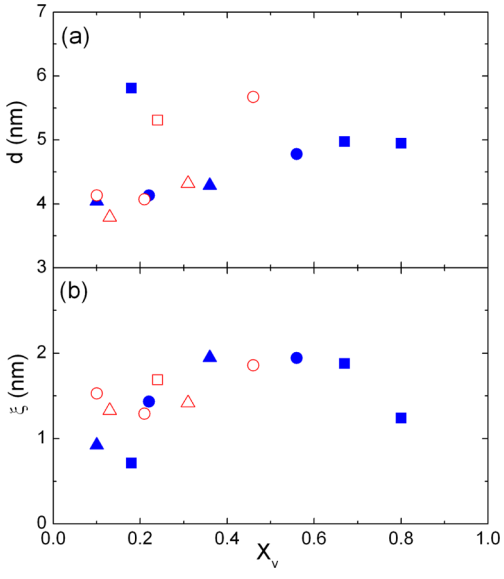

Figure 10. Characteristic lengths for the ion-rich domains from the TS model: (a) characteristic distance between domains and (b) distance over which the domains are correlated. Results are shown for the LGD (short, ■; medium, ▲; and long, ●) and the HGD (short, □; medium, △; and long, ○) series.

DISCUSSION

Our results show that the graft polymers phase separate to form fluorous domains in a polystyrene matrix, consistent with the low volume fraction of PVDF in these samples. This is in contrast to the diblock samples studied previously[12] which exhibited morphology consistent with PS domains in a fluorous matrix at low PS volume fractions and a lamellar structure of alternating fluorous and PS domains when the volume fractions were roughly equivalent. We have shown here that the size of the fluorous domains depends on the graft density, but not on graft chain length, with some dependence on the charge content, and that the LGD samples are generally less ordered than the HGD samples, consistent with a higher degree of crystallinity in the former samples. In the following sections, we will discuss the impact of these morphological differences on the macroscopic properties of both the graft and diblock materials. Data for the diblock materials were reported previously.[10,11,34]

Water Content. Figure 11 compares the swelling in samples of different charge content for the two series. In order to directly compare how much the PS matrix swells, this figure plots the water uptake as a function of the IEC, with both quantities expressed relative to the mass of the PS matrix, where the PS matrix includes either partially sulfonated or fully sulfonated PS depending on the sample. The traditional form of this graph, the water uptake of the sample plotted as a function of the IEC based on the total mass of the sample, is shown in Figure S2 of the Supporting Information. The general trend, that the water uptake increases as the IEC increases, is the same in both representations. Comparing the swelling of the PS matrix allows us to see clear differences between the samples and directly study the impact of morphology.

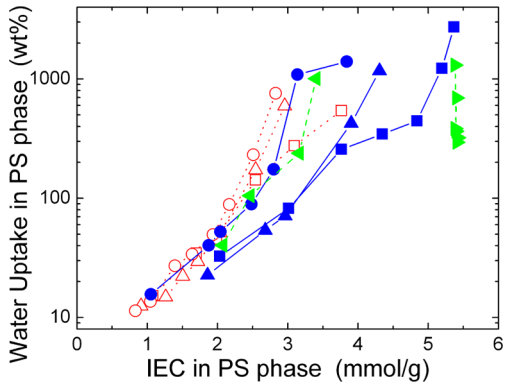

Figure 11. Swelling of the polystyrene phase for graft and diblock copolymer membranes. Results are shown for LGD (short, ■; medium, ▲; and long, ●), HGD (short, □; medium, △; and long, ○), fully sulfonated diblocks (▶), and partially sulfonated diblocks (◀).

dx.doi.org/10.1021/ma402008b | Macromolecules 2013, 46, 9676−9687

At low IEC, swelling of the HGD samples and the long LGD samples is very similar, while the short and medium LGD samples clearly swell less. At high IEC, further differences between these samples are apparent. These results can be interpreted by assuming that two parameters impact the swelling: the PVDF content and its crystallinity. Within each series, the samples with shorter graft lengths have higher PVDF content. In particular, is clear that the extreme swelling at high IEC decreases systematically with side chain length, and we attribute this to the increase in PVDF content.

To isolate the effects of crystallinity, we examine the data for samples with short side chains from the LGD series (■) and HGD series (□). These two sets of samples have very similar PVDF ratios and side chain lengths. The fact that the LGD series has a lower water content for similar charge content can be attributed to the fact that it is partially crystalline; backbone crystallinity is known to increase the elasticity of a polymer membrane.[35−37]

The PS phase of the partially sulfonated diblock samples (◀) was not crystalline[12] and exhibited swelling similar to the HGD samples. The charge content in the PS phase of all the fully sulfonated diblock samples (▶) is the same, as expected. Four of the six samples also have the same water uptake; the two outliers are the samples with the lowest and highest average sample IEC.

Conductivity. Figure 12 compares the conductivity of the graft and diblock samples plotted as a function of water

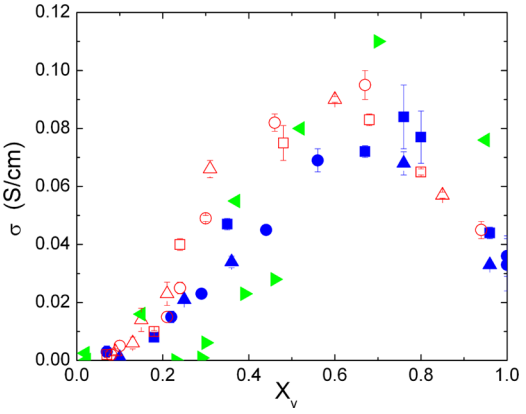

Figure 12. Dependence of the conductivity of the graft and diblock polymer membranes on water content. Results are shown for LGD (short, ■; medium, ▲; and long, ●), HGD (short, □; medium, △; and long, ○), fully sulfonated diblocks (▶), and partially sulfonated diblocks (◀).

content. The traditional form of this graph, conductivity plotted as a function of the mass-based IEC, is included in the Supporting Information as Figure S3. As shown by other authors,[38] expressing conductivity in terms of volume-based parameters, in particular the volume fraction of sample that is conducting, leads to a higher correlation between conductivity of different samples. We see that all data show some similar characteristics. Conductivity is low at low water content, increases to a maximum around $X_v \approx 0.7$, and then decreases. As described by other authors, low conductivity at low water content is attributed to high tortuosity, resulting in low proton mobility, while a decrease at high water content is attributed to decrease in proton concentration.[39] Comparing the two graft series, we observe that the higher graft density samples have a higher conductivity at lower water contents and that the conductivity of the LGD samples peaks at a higher water content. Data for the partially sulfonated diblocks lie between these two curves. Data for the fully sulfonated diblocks are generally below the others. We can gain insight into these differences by discussing the data in terms of the conductivity of porous materials.

In a porous material consisting of a conducting phase and a supporting matrix, the conductivity of the material is described in terms of the porosity of the medium ε and its tortuosity τ (see for example ref 40):

$$\sigma = \frac{\varepsilon}{\tau}\sigma_0 \tag{9}$$

where σ_0 is the conductivity of the conducting phase. The porosity represents the fraction of the volume where conductivity occurs. If we assume all conductivity occurs in the water phase, then we can use X_v for this parameter. The tortuosity is a parameter of the membrane and describes the reduction in conductivity due to the nature of the path along which conduction occurs.

In this picture, σ_0 is the bulk conductivity of the water phase and is to first order simply proportional to the proton concentration in the water phase.[23,40,41] We can determine the proton concentration c^+ from the IEC and water uptake

$$c^+ = \frac{\text{IEC}\ \rho_w}{\text{water uptake}} \tag{10}$$

where ρ_w is the density of water. This expression for c^+ assumes that all the absorbed water is in the conducting phase and that the sulfonic acid groups are fully dissociated. A plot of proton concentration for samples of different water content (Figure 13a) shows proton concentration decreasing in all samples. In particular, data for the two graft series are very consistent with no evidence of an increased proton concentration in either series. There are profound differences in the data for the fully sulfonated diblocks; we speculate that the low polystyrene content of these samples leads to isolated ion-rich domains where there is some uncertainty the measurements.

Rearranging eq 9 provides an expression of the tortuosity:

$$\tau = \frac{\varepsilon\sigma_0}{\sigma} \tag{11}$$

We can compare the tortuosity of samples with different morphology by plotting $X_v c^+/\sigma$ as a function of the water content. Results for the four series are shown in Figure 13b. The general behavior is the same; the tortuosity decreases for all samples as the water content increases and the water phase becomes more continuous. Comparing the two series of graft copolymers, we find that the tortuosity is slightly larger in the LGDs in the region where we see differences between the conductivity for the two series, i.e., X_v 0.2. These are the samples that are partially crystalline and more disordered. We conclude that the crystallinity and/or lower degree of phase separation has impacted the conductivity by reducing the connectivity of the conducting phase. There is a large deviation from the general behavior for samples from the fully sulfonated diblock series at low water content, presumably due to the disconnected SPS regions in these samples at low water content. The partially sulfonated diblock series has the lowest tortuosity; recall that this series is characterized by a lamellar structure guaranteeing well-connected water channels over a wide range of water content. It is interesting to note that the tortuosity reaches a constant value in all samples for water

dx.doi.org/10.1021/ma402008b | Macromolecules 2013, 46, 9676−9687

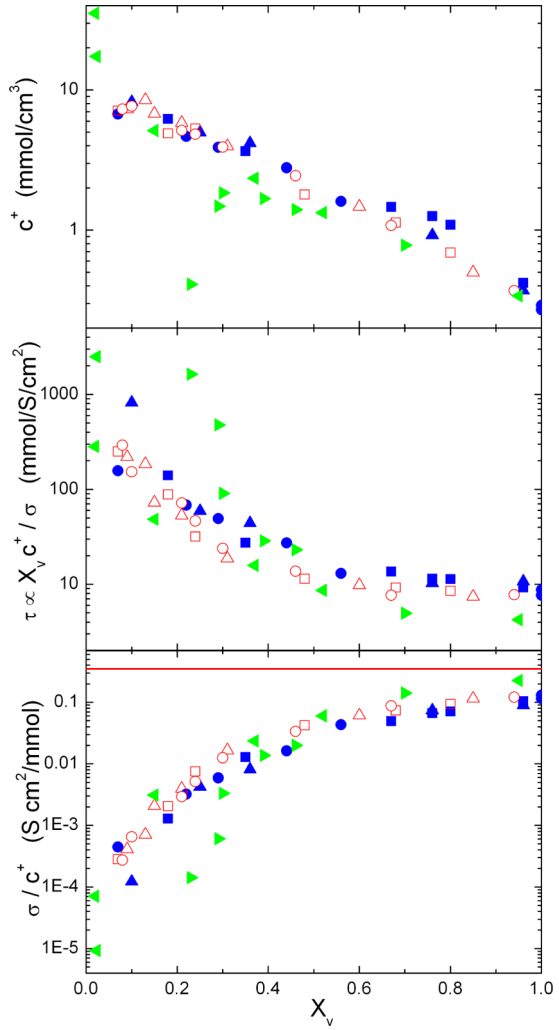

Figure 13. (a) Proton concentration and (b) tortuosity in the conducting phase of the graft and diblock polymer membranes decrease with water content. (c) Normalized conductivity of the conducting phase. Results are shown for LGD (short, ■; medium, ▲; and long, ●, side chains), HGD (short, □; medium, △; and long, ○, side chains), fully sulfonated diblocks (▶), and partially sulfonated diblocks (◀).

contents greater than 60%. For the LGD and HGD series, this correlates with the region where we start to see deviations of the data from the proposed model.

Some materials show a percolation threshold in the proton conductivity[23,40,41]

$$\sigma = (\varepsilon - \varepsilon_0)^t \sigma_0 \quad (12)$$

Figure 13c shows a plot of the normalized conductivity, σ/c^+, as a function of water content. The LGD and HGD graft series and the partially sulfonated diblock series show similar normalized conductivity, with a percolation threshold near $X_v = 0$, as is observed for Nafion when the water content is changed by varying the humidity of the sample environment.[42] The fully sulfonated diblock series has a finite percolation threshold, as expected for a sample containing <50 vol % water and confirming the picture of a material that does not have sufficient connection between regions of conducting phase for sufficient conduction paths at low water content. Finite percolation thresholds are also observed in SPEEK membranes and some radiation grafted materials.[23] The red line on the data represents the value expected for the normalized conductivity calculated using the mobility of protons in pure water. As commented previously,[8] at high water content, the normalized conductivity approaches but remains below the value expected for pure water. This implies that even at high water content where the sample is mostly water, the proton mobility is still affected by the polymer.

CONCLUSIONS

We have studied the morphology of a diverse set of samples from two series of an ionic random graft copolymer P(VDF-*co*-CTFE)-*g*-SPS. The series differ in graft density; the LGD series has a graft density of 1.7%, and the HGD series has a graft density of 2.3−2.7%. Previously, we had shown that the PVDF backbone of the LGD series was partially crystalline. Samples in each series were synthesized to have either short, medium, or long PS grafts attached to the PVDF backbone. The PS was sulfonated from 0 to 100%. SAXS measurements were made on dry samples, and SANS measurements were made on samples hydrated with four water compositions: H_2O, D_2O, a 30:70 mixture of D_2O:H_2O, and a 60:40 mixture of D_2O:H_2O.

Scattering studies reveal a morphology consisting of a disordered, partially phase-separated system, with two characteristic features. By comparing spectra for samples hydrated in water of different isotopic composition, we confirmed a morphology consisting of PVDF domains in a partially sulfonated PS matrix with aggregation of ion-rich domains within the matrix. The data were interpreted by fitting the Kinning−Thomas model to the PVDF peak and the Teubner−Strey model to the peak associated with the ion-rich domains. We explored other models but found that this combination provided the best fit to the data and resulted in a set of parameters consistent with the main features of the data. Results for the average size, distance of closest approach, and volume fraction of the PVDF domains and the characteristic separation of the ion-rich domains were obtained.

We found that the size of the core of the PVDF domains is independent of both the PS graft chain length and the hydration of the sample but depends on the graft number density, with samples with lower graft number density, and consequently a greater distance between graft points, having larger domains. The size of the domains is highest in the unsulfonated and fully sulfonated samples, decreasing slightly at intermediate degrees of sulfonation.

The minimum separation between the PVDF domains was greater than twice the radius of the domains, indicating that the packing of the domains is impeded, perhaps by a shell of PS chains. The thickness of this shell is larger for samples with longer side chains and is highest in unsulfonated and fully sulfonated samples, decreasing at intermediate degrees of sulfonation. The minimum separation increased with water content by amounts consistent with measurements of the water uptake, indicating consistency between microscopic and macroscopic swelling in these materials.

We estimated the degree of phase separation between fluorous and polystyrene components from the hard-sphere volume fraction of the cores of the fluorous domains and by comparing the volume of the cores to the total volume of PVDF in each sample. Crystallinity in the LGD series leads to a significantly lower degree of phase separation. Phase separation is highest in the HGD series with longer side chains, consistent with what is seen in conventional copolymers where the interaction energy depends on the degree of polymerization. In

dx.doi.org/10.1021/ma402008b | *Macromolecules* 2013, 46, 9676−9687

addition, the degree of phase separation is highest in the unsulfonated and fully sulfonated samples. In these cases, the fluorous domains are embedded in a uniform continuous phase of either unsulfonated or fully sulfonated polystyrene. In the partially sulfonated samples, we believe that phase separation of PVDF and PS is reduced because it is in competition with aggregation of the acid groups along the side chains.

We looked for evidence of impact of details of the morphology on two major considerations for use of proton conducting membranes in PEMFCs: water content and conductivity. We compared results for the two graft series with two series of diblock copolymers studied previously. The crystallinity can reduce the swelling of the membranes in water; partially crystalline samples with PVDF content >25% swell less than noncrystalline or PVDF poor samples. However, the conductivity path is more tortuous in these samples, consistent with the fact that the phase separation is more limited. Samples with a continuous PS phase do not exhibit a significant percolation threshold of water content required for conduction to occur—the only architecture to exhibit a percolation threshold was the low PS content diblock series where the PS exists as isolated domains in the dry state. It is remarkable the similarities in water uptake and conductivity values for membranes of radically different morphology, particularly when volume-based quantities are compared. We conclude that details of the morphology—size of the fluorous domains or their organization, for example—do not have a direct impact on swelling or conductivity. But the ability to control the water uptake through crystallinity of the fluorous domain or the amount of PVDF in the sample has a large impact—ultimately—on the conductivity. The ability to control water uptake through control of molecular architecture is thus a key feature in design of these materials.

■ ASSOCIATED CONTENT

Supporting Information

Definitions of some of the terms used in the text, details of calculations and models used in the fits, results from contrast matching experiments, tables of parameters for the samples, and supplemental figures. This material is available free of charge via the Internet at http://pubs.acs.org.

■ AUTHOR INFORMATION

Corresponding Author

*E-mail frisken@sfu.ca; Ph +1 778 782 5767; Fax +1 778 782 3592 (B.J.F.).

Notes

The authors declare no competing financial interest.

■ ACKNOWLEDGMENTS

We gratefully acknowledge Dr. Olivier Diat of the CEA for his help with SANS experiments and many useful discussions. We acknowledge the support of the Institut Laue-Langevin, France, in providing the neutron facilities used in this work (proposal numbers 9-11-1257 and 9-11-1493) and thank Dr. L. Porcar for his help with the neutron scattering experiments. We acknowledge the support of the National Institute of Nanotechnology of the National Research Council of Canada and the Adolphe-Merkle Institute, Switzerland, in providing X-ray facilities and Mr. S. Launspach and Dr. C. Judd, respectively, for their help with experiments at these facilities. This research has been supported by NSERC Canada.

■ REFERENCES

(1) Hickner, M. A.; Ghassemi, H.; Kim, Y. S.; Einsla, B. R.; McGrath, J. E. *Chem. Rev.* **2004**, *104*, 4587−4612.
(2) Mauritz, K. A.; Moore, R. B. *Chem. Rev.* **2004**, *104*, 4535−4585.
(3) Yang, Y.; Holdcroft, S. *Fuel Cells* **2005**, *5*, 171−186.
(4) Elabd, Y. A.; Hickner, M. A. *Macromolecules* **2011**, *44*, 1−11.
(5) Wang, X.; Goswami, M.; Kumar, R.; G. Sumpter, B.; Mays, J. *Soft Matter* **2012**, *8*, 3036−3052.
(6) Nieh, M.-P.; Guiver, M. D.; Kim, D. S.; Ding, J.; Norsten, T. *Macromolecules* **2008**, *41*, 6176−6182.
(7) Tsang, E. M. W.; Zhang, Z.; Shi, Z.; Soboleva, T.; Holdcroft, S. *J. Am. Chem. Soc.* **2007**, *129*, 15106−15107 .
(8) Tsang, E. M. W.; Zhang, Z.; Yang, A. C. C.; Shi, Z.; Peckham, T. J.; Narimani, R.; Frisken, B. J.; Holdcroft, S. *Macromolecules* **2009**, *42*, 9467−9480.
(9) Yang, A. C. C.; Narimani, R.; Zhang, Z.; Frisken, B.; Holdcroft, S. *Chem. Mater.* **2013**, *25*, 1935−1946.
(10) Shi, Z.; Holdcroft, S. *Macromolecules* **2004**, *37*, 2084−2089.
(11) Shi, Z.; Holdcroft, S. *Macromolecules* **2005**, *38*, 4193−4201.
(12) Rubatat, L.; Shi, Z.; Diat, O.; Holdcroft, S.; Frisken, B. J. *Macromolecules* **2006**, *39*, 720−730.
(13) Zhang, Z.; Chalkova, E.; Fedkin, M.; Wang, C.; Lvov, S. N.; Komarneni, S.; Chung, T. C. M. *Macromolecules* **2008**, *41*, 9130−9139.
(14) Chu, B.; Hsiao, B. S. *Chem. Rev.* **2001**, *101*, 1727−1762.
(15) Gebel, G.; Diat, O. *Fuel Cells* **2005**, *5*, 261−276.
(16) Narimani, R. Morphological Studies of Ionic Random Graft Copolymers Based on Scattering Techniques. Ph.D. Thesis, Simon Fraser University, Burnaby BC, 2012.
(17) These values have been calculated using the online NIST SLD calculator (www.ncnr.nist.gov/resources/sldcalc.html), assuming densities of 1.78 mg/mL for PVDF and 1.05 mg/mL for PS.
(18) Kinning, D. J.; Thomas, E. L. *Macromolecules* **1984**, *17*, 1712−1718.
(19) Percus, J. K.; Yevick, G. J. *Phys. Rev.* **1958**, *110*, 1−13.
(20) Schwab, M.; Stühn, B. *Colloid Polym. Sci.* **1997**, *275*, 341−351.
(21) Teubner, M.; Strey, R. *J. Chem. Phys.* **1987**, *87*, 3195−3200.
(22) Kotlarchyk, M.; Chen, S.-H. *J. Chem. Phys.* **1983**, *79*, 2461−2469.
(23) Balog, S.; Gasser, U.; Mortensen, K.; Ben Youcef, H.; Gubler, L.; Scherer, G. G. *J. Membr. Sci.* **2011**, *383*, 50−59.
(24) Gebel, G.; Lambard, J. *Macromolecules* **1997**, *30*, 7914−7920.
(25) Debye, P.; Bueche, A. M. *J. Appl. Phys.* **1949**, *20*, 518−525.
(26) Doll, W.; Lando, J. *Macromol. Sci.* **1970**, *B4*, 309−329.
(27) Hasegawa, R.; Takahashi, Y.; Tadokoro, H. *Polym. J.* **1972**, *3*, 600−610.
(28) Kinning, D. J.; Thomas, E. L.; Fetters, L. J. *J. Chem. Phys.* **1989**, *90*, 5806−5825.
(29) Visser, S. A.; Cooper, S. L. *Macromolecules* **1991**, *24*, 2584−2593.
(30) Hamley, I. *The Physics of Block Copolymers*; Oxford University Press: New York, 1999.
(31) Kim, S. Y.; Park, M. J.; Balsara, N. P.; Jackson, A. *Macromolecules* **2010**, *43*, 8128−8135.
(32) Park, M. J.; Balsara, N. P. *Macromolecules* **2008**, *41*, 3678−3687.
(33) Hall, L. M.; Seitz, M. E.; Winey, K. I.; Opper, K. L.; Wagener, K. B.; Stevens, M. J.; Frischknecht, A. L. *J. Am. Chem. Soc.* **2012**, *134*, 574−587.
(34) Shi, Z. Q. Synthesis and Characterization of Proton-conducting, Fluorine-containing Block Copolymers. Ph.D. Thesis, Simon Fraser University, Burnaby BC, 2004.
(35) Gebel, G.; Aldebert, P.; Pineri, M. *Macromolecules* **1987**, *20*, 1425−1428.
(36) Schmidt-Rohr, K.; Chen, Q. *Nat. Mater.* **2008**, *7*, 75−83.
(37) Uehara, H.; Kakiage, M.; Sekiya, M.; Yamagishi, T.; Yamanobe, T.; Nakajima, K.; Watanabe, T.; Nomura, K.; Hase, K.; Matsuda, M. *Macromolecules* **2009**, *42*, 7627−7630.
(38) Kim, Y. S.; Pivovar, B. S. *Annu. Rev. Chem. Biomol. Eng.* **2010**, *1*, 123−148.

(39) Peckham, T. J.; Schmeisser, J.; Rodgers, M.; Holdcroft, S. *J. Mater. Chem.* **2007**, *17*, 3255−3268.
(40) Pisani, L.; Valentini, M.; Hofmann, D. H.; Kuleshova, L. N.; D'Aguanno, B. *Solid State Ionics* **2008**, *179*, 465−476.
(41) Knauth, P.; E, S.; Donnadio, A.; Casciola, M.; Di Vona, M. L.
(42) Rubatat, L. Nouveau modèle structural des membranes Nafion, polymère de référence pour l'application pile à combustible basse température. Ph.D. Thesis, l'Université Joseph Fourier, Grenoble, 2003.